

# Internal alignment of the *BABAR* silicon vertex tracking detector

*D. Brown<sup>a</sup>, A. Gritsan<sup>b</sup>, D. Roberts<sup>c</sup>*

<sup>a</sup> *Lawrence Berkeley National Laboratory, Berkeley, CA, USA*

<sup>b</sup> *Johns Hopkins University, Baltimore, MD, USA*

<sup>c</sup> *University of Maryland, College Park, MD, USA*

## Abstract

The *BABAR* Silicon Vertex Tracker (SVT) is a five-layer double-sided silicon detector designed to provide precise measurements of the position and direction of primary tracks, and to fully reconstruct low-momentum tracks produced in  $e^+e^-$  collisions at the PEP-II asymmetric collider at Stanford Linear Accelerator Center. This paper describes the design, implementation, performance and validation of the *local alignment* procedure used to determine the relative positions and orientations of the 340 Silicon Vertex Tracker wafers. This procedure uses a tuned mix of lab-bench measurements and complementary in-situ experimental data to control systematic distortions. Wafer positions and orientations are determined by minimizing a  $\chi^2$  computed using these data for each wafer individually, iterating to account for between-wafer correlations. A correction for aplanar distortions of the silicon wafers is measured and applied. The net effect of residual mis-alignments on relevant physical variables evaluated in special control samples is presented.

## 4.1 Introduction

This section describes the procedure developed and used for the *BABAR* Silicon Vertex Tracker local alignment. Our procedure uses track data recorded during normal *BABAR* running, filtered and prescaled to produce a fixed sample that roughly uniformly illuminates all the wafers, and constrains all the local alignment degrees of freedom in a statistically independent and systematically complete way. Tracks are fit using Silicon Vertex Tracker hits and constrained using a subset of Drift Chamber and beam energy information selected to not impose any significant systematic bias on the local alignment. To avoid statistical bias, we select an independent subset of information from each track. We combine track-based information with direct measurements of the relative positions and orientations of Si wafers made during detector construction, resulting in a statistically correct and systematically robust measure of the consistency ( $\chi^2$ ) of a wafer's position and orientation within the detector. We use an iterative technique to determine the relative wafer positions that minimize

the  $\sum \chi^2$  of all wafers. The resultant local alignment is then validated against several possible systematic effects. Each of these functions is described in detail in the following sections.

The *BABAR* Silicon Vertex Tracker local alignment procedure is written in C++ and runs in the standard *BABAR* reconstruction and analysis framework, and uses standard *BABAR* data persistence [1]. The alignment results are stored in the *BABAR* conditions database [2]. Tcl/Tk [3] are used to build the user interface and script job control.

## 4.2 The silicon vertex tracker

The *BABAR* Silicon Vertex Tracker (SVT) was designed to provide precise reconstruction of charged-particle trajectories and decay vertices near the interaction region, as required by diverse *BABAR* physics requirements. Because of the relatively poor  $z$  resolution provided by the DCH stereo wire measurement, the SVT also provides the track  $z$  position and  $\theta$  angle measurement at the DIRC and EMC.

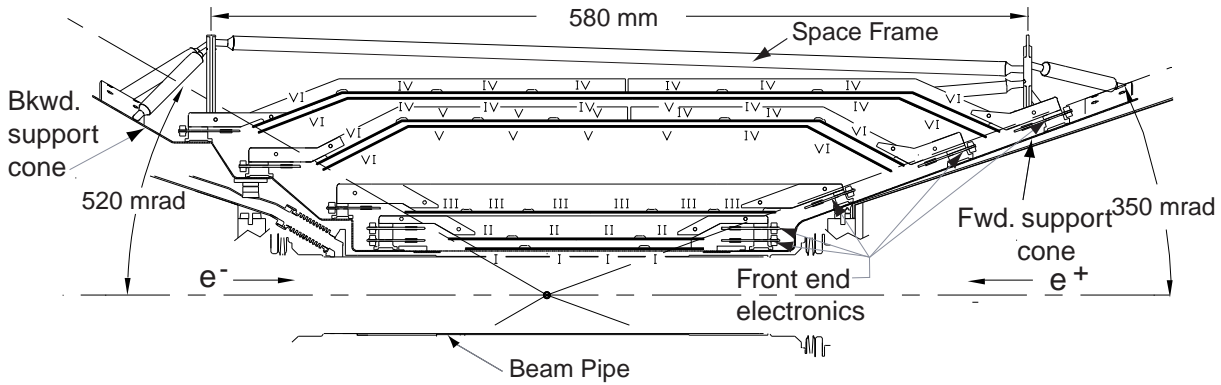


Fig. 4.1: Longitudinal section of the *BABAR* SVT. The roman numbers label the six different types of wafers

The SVT is composed of 340 separate Si wafers, arranged in 5 co-axial roughly cylindrical layers, see Fig. 4.1. Each layer is composed of between 6 and 18 planar modules, arranged symmetrically around the  $z$  axis, held in place by a rigid carbon-fibre frame. Each module is in turn composed of between 4 and 8 individual Si wafers, glued together along supporting carbon-fibre ribs. See Table 4.1 for geometric parameters of each layer.

There are six different wafer shapes, including a trapezoidal shape used to form the arch modules discussed below. The smallest wafers are  $4.3 \times 4.2 \text{ cm}^2$ , and the largest are  $6.8 \times 5.3 \text{ cm}^2$ .

The modules of the inner three layers are straight, while the modules in layers 4 and 5 are arch-shaped. This design was chosen to minimize the amount of material while increasing the crossing angle for particles originating from the interaction region. The modules in the inner three layers are tilted by  $5^\circ$ , allowing an overlap region between adjacent modules, see Fig. 4.2. This arrangement is advantageous for alignment and provides full azimuthal coverage. The outer layers cannot be tilted because of the arch geometry. To have an overlap in the azimuthal direction and to avoid gaps, the outer two layers are divided into two sub-layers (4a, 4b, 5a, 5b) which are placed at slightly different radii.

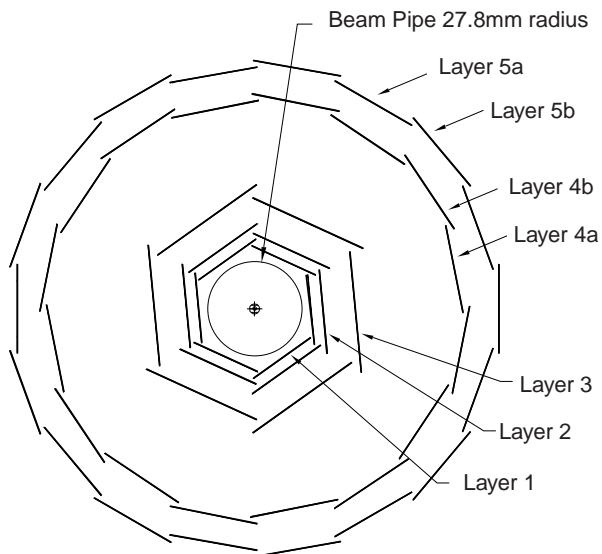


Fig. 4.2: Transverse section of the *BABAR* SVT

Table 4.1: Geometric parameters of five SVT layers comprised of 340 silicon wafers. The radial range for layers 4 and 5 includes the radial extent of the arched sections.

Layer	Wafers per module	Modules per layer	Radius (mm)	z-strip length (mm)	$\phi$ -strip length (mm)
1	4	6	32	40	82
2	4	6	40	48	88
3	6	6	54	70	128
4	7	16	91–127	104	224
5	8	18	114–144	104	265

The strips on opposite sides of each wafer are oriented orthogonally to each other: the  $\phi$  measuring strips

run parallel to the beam and the  $z$  measuring strips are oriented transversely to the beam axis.

In this note we refer to the *local* wafer coordinate system, described by a right-handed Cartesian coordinates  $uvw$  defined uniquely for every wafer. The  $w$  axis is defined as the normal direction to the nominal Si plane of the wafer, roughly outwards from the IP  $\hat{w} \cdot \hat{\rho} > 0$ . The  $u$  axis is defined to lie in the plane of the Si wafer pointing in the direction of increasing global  $\phi$  as  $\hat{u} \cdot \hat{w} = 0$  and  $\hat{u} \cdot \hat{z} = 0$ . The  $v$  coordinate is defined to lie in the plane of the Si wafer, orthogonal to  $\hat{u}$  and  $\hat{w}$ , pointing roughly in the direction of the global  $z$  axis  $\hat{v} \cdot \hat{z} > 0$ . The local wafer coordinate system origin is defined as the geometric centre of the wafer.

We define  $\alpha_u$ ,  $\alpha_v$  and  $\alpha_w$  as small right-handed rotations about  $\hat{u}$ ,  $\hat{v}$  and  $\hat{w}$  respectively, in units of radians. Hits reconstructed in the SVT using the strips parallel to  $\hat{v}$  are referred to as  $u$  hits, as that is the dimension they constrain. Similarly hits using strips parallel to  $\hat{u}$  are referred to as  $v$  hits.

An optical survey of the SVT on its assembly jig indicated that the global error in placement of wafers with respect to design was a few hundred microns. Subsequently, the SVT was disassembled, shipped to SLAC, and reassembled on the PEP-II magnets.

The SVT support structure is a rigid body made from two carbon-fibre cones, connected by a space frame, also made of carbon-fibre epoxy laminate. The SVT is mounted on the PEP-II beampipe and its assembly allows for relative motion of the support structures with respect to the dipole magnets of the PEP-II. The mounting of the SVT independently of *BABAR* allows for movement between the SVT and the rest of the detector. During operation the SVT is cooled to remove the heat generated by the electronics and is kept in the humidity controlled environment.

### 4.3 Goals and requirements of the SVT local alignment

The goal of the SVT local alignment is to provide estimates of the relative positions and orientations of the constituent Si wafers such that the residual misalignments contribute negligibly to the final uncertainty in the physics quantities extracted using the tracks reconstructed in the SVT. We consider each Si wafer as an independent rigid body located and oriented near its nominal construction position and orientation. The local alignment must provide 3 displacements ( $\delta_u$ ,  $\delta_v$ ,  $\delta_w$ ) and 3 rotations ( $\alpha_u$ ,  $\alpha_v$ ,  $\alpha_w$ ) which describe the true position and orientation of the wafer with respect to that nominal, expressed in the local wafer coordinate frame.

This gives a total of 2040 parameters which must be determined by the local alignment procedure, with 6 redundant global degrees of freedom. As described in

detail in Section 4.9, we also model the curvature of the inner 3 layers of wafers in the  $u$ - $w$  plane, adding 84 additional parameters. The estimated Lorentz shift in the position of  $u$  hits induced by *BABAR*'s solenoid is accounted for in the SVT hit reconstruction. Any difference between this estimate and the actual Lorentz shift is absorbed into the  $\delta_u$  parameter.

As described in Section 4.2, we observed some slow internal motion of the SVT wafers related to humidity expansion in the module support, and due to stress changes during periods of active access to the detector and during normal operation. The alignment procedure must therefore be able to operate on a small subset of the *BABAR* data, and the procedure must be efficient. The rarest process used in the local alignment turns out to be cosmic rays, whose rate is independent of beam luminosity. Consequently, we define a local alignment data sample based on a fixed calendar period of around 2 weeks. Computing the alignment constants should take no more than 24 hours.

A track passing through the full SVT will generally generate 2 hits (1  $u$  and 1  $v$ ) in each of 5 layers. As a track's trajectory is well-described as a 5-parameter helix [4], a single track constrains 5 degrees of freedom. Most of these constraints are, however, on the global, not local alignment.

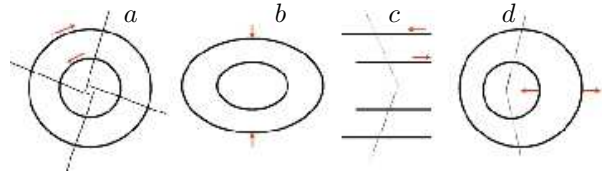


**Fig. 4.3:** We show some of the large-scale systematic alignment distortions possible in a multi-wafer cylindrical Si detector that affect the relative position of nearby wafers only to second order. The effects shown have been scaled by a factor of 1000 compared to the maximum distortion requirements of the local alignment described in Section 4.3. (a) shows a *radial distortion (curl)*, (b) *elliptical distortion*, (c) *telescope*, (d) *axial twist*.

Furthermore, because tracks scatter as they pass through material, the most statistically powerful local alignment constraints will be on the relative positions of wafers in adjacent layers. Similarly, lab-bench measurements of relative wafer positions are useful only for nearby wafers, as mechanical and thermal stress uncertainties grow quickly with relative distance. This raises the risk that a local alignment procedure based on tracks and lab-bench measurements might correctly constrain the relative position of nearby wafers, but could produce large-scale distortions, such as are shown in Fig. 4.3.

In Table 4.2 we summarize the main systematic distortions in a system with cylindrical geometry, such

as SVT. If uncorrected, these distortions would produce unacceptable biases in physics distributions.

**Table 4.2:** Main systematic distortions in a system with cylindrical geometry and multiple layers. Distortions in  $r$ ,  $z$ , and  $\phi$  are considered as a function of these coordinates. The potential impact of these distortions on physics results is indicated.

	$\Delta r$	$\Delta\phi$	$\Delta z$
vs. $r$	<b>Radial expansion</b> Distance scale	<b>Curl</b> Charge asymmetry	<b>Telescope</b> z momentum
vs. $\phi$	<b>Elliptical</b> Vertex mass	<b>Clamshell</b> Vertex displacement	<b>Skew</b> z momentum
vs. $z$	<b>Bowing</b> Total momentum	<b>Twist</b> CP violation	<b>z expansion</b> Distance scale

A fundamental requirement of the SVT local alignment procedure is to avoid global systematic distortions. To estimate specific requirements on how well we must determine of the different local alignment parameters, we consider the implications of a subset of relevant *BABAR* physics measurements.

To observe  $CP$  violation in  $\Upsilon(4S) \rightarrow B^0\bar{B}^0$ , the SVT must be able to precisely measure the roughly  $250 \mu\text{m}$  average separation between the  $B$  meson decay vertices. A full detector simulation study [5] showed this requires an average resolution of no worse than  $10 \mu\text{m}$  for  $u$  hits and  $20 \mu\text{m}$  for  $v$  hits. To insure that the local alignment does not statistically dilute or systematically bias these measurements, we require the residual local alignment uncertainty not contribute more than 5% in quadrature to the resolution. This implies knowing  $\delta_u$  to roughly  $2 \mu\text{m}$ ,  $\delta_v$  to roughly  $5 \mu\text{m}$ , and  $\alpha_w$  to roughly  $2 \mu\text{rad}$ .

To make competitive measurements of the  $\tau$  lepton and  $B$  meson lifetimes, the absolute distance scale provided by the SVT measurements must be understood to better than 1 part in 1000. This implies a maximum residual uncertainty on  $\delta_w/\rho$  of  $1/1000$ , where  $\rho$  is the average transverse radius of the layer. For layer 3 this implies determining  $\delta_w$  better than  $10 \mu\text{m}$ . Similarly,  $\delta_v/z$  must be known better than  $1/100$ , implying constraining  $\delta_v$  to  $5 \mu\text{m}$  over the length of the detector.

<sup>1</sup>To date, one iteration of the local alignment pre-selection has been sufficient to select an unbiased sample.

## 4.4 The local alignment event sample

The data used to perform the SVT local alignment are selected from those collected during normal physics running of the *BABAR* detector. The *BABAR* physics trigger accepts a mix of events including hadronic decays of the  $\Upsilon(4S)$  into  $B$  mesons and other hadrons,  $e^+e^- \rightarrow \mu^+\mu^-$  events,  $e^+e^- \rightarrow e^+e^-$  events,  $\tau$  decays,  $2\text{-}\gamma$  events, and some cosmic rays. Initially the *BABAR* cosmic-ray trigger required the tracks to pass within a few centimetres of the nominal interaction point (IP).

The local alignment data sample is pre-selected during prompt event reconstruction. Final track and Silicon Vertex Tracker hit selections are used to define a statistically independent sample that covers all the local alignment degrees of freedom. Data samples dedicated to local alignment processing and study are stored in a version of the standard *BABAR* event format optimized for the local alignment. These samples are the input to the minimization procedure described in the next section. Details of the event and track selection and preparation, SVT hit selection, and local alignment data formats are presented in the following subsections, and shown graphically in Fig. 4.4.

### 4.4.1 Event preselection

A preselection of events of eventual interest to the local alignment procedure is integrated into the *BABAR prompt reconstruction* procedure that runs shortly after the events are recorded [6].

All triggered events are first passed through a minimal background rejection procedure which removes most beam-gas interactions and scales down  $e^+e^- \rightarrow e^+e^-$  interactions [6]. A pseudo-random prescaling is then applied to  $e^+e^- \rightarrow e^+e^-$ ,  $e^+e^- \rightarrow \mu^+\mu^-$  and cosmic-ray triggers, which results in a roughly uniform illumination of the detector.

Tracks in preselected events are then found using standard road-based pattern recognition algorithms in both the *BABAR* Drift Chamber (DCH) and the SVT and fit using a Kalman filter algorithm [4] that accounts for differing hit resolutions, detector material, and magnetic field inhomogeneities. Tracks found in the DCH (SVT) are extrapolated into the SVT (DCH) respectively, and hits consistent with the Kalman fit are added. Prompt track reconstruction uses the most recent local alignment parameters available at the time of processing. If, at the end of the local alignment procedure, we observe a large change in local alignment that might affect initial event selection or track reconstruction, we repeat the entire local alignment procedure starting with preselection, using the updated local alignment parameters, and iterate as necessary<sup>1</sup>.

Preselected events are written to a dedicated calibration *stream* (file). The calibration stream persists events in the standard *BABAR mini-dst* event format [1], which records the reconstructed tracks and their associated hits. In addition to other information, the SVT hit storage format records the wafer-frame *local* centroid of the hit.

#### 4.4.2 Event categorization and final selection

On readback, the SVT and DCH hits of all the previously reconstructed tracks in the calibration stream events are reconstituted from their local positions using the current local alignment and calibration, and the full Kalman filter fit of the track is rebuilt. Well-measured tracks are then preselected to be used in final event selection and classification.

To insure a reliable momentum measurement, only tracks with at least 10 DCH hits, and at least 2 *v* and 3 *u* SVT hits<sup>2</sup> are selected for use in the local alignment. To minimize multiple scattering effects, we also require a transverse momentum of at least 1 GeV. To cut down on background from secondary (material) interaction products, we accept only tracks whose point of closest approach to the *BABAR* *z* axis is within 1.5 cm of the IP in the  $\hat{\rho}$  direction and inside  $-7$  cm and  $+9$  cm of the IP in the  $\hat{z}$  direction.

Events are categorized and finally selected based on the multiplicity and properties of their selected tracks. We currently define four categories of events in the local alignment;  $e^+e^- \rightarrow \mu^+\mu^-$ ,  $e^+e^- \rightarrow e^+e^-$ , cosmic ray, and ‘normal’. The definitions and selections of these categories is described below.

Events with exactly two selected tracks are tested as potential  $e^+e^- \rightarrow \mu^+\mu^-$  or  $e^+e^- \rightarrow e^+e^-$  events. Tracks in  $e^+e^- \rightarrow \mu^+\mu^-$  candidates are required to have associated calorimeter signals consistent with a minimum-ionizing particle. Tracks in  $e^+e^- \rightarrow e^+e^-$  candidates are required to have associated calorimeter energy deposition consistent with the reconstructed track momentum. Both  $e^+e^- \rightarrow \mu^+\mu^-$  and  $e^+e^- \rightarrow e^+e^-$  events are required to have a total energy (computed from track momentum) consistent with the known combined energy of the initial  $e^+e^-$  beams, and to be back-to-back in the  $\hat{\rho}$  plane.

Candidate  $e^+e^- \rightarrow \mu^+\mu^-$  and  $e^+e^- \rightarrow e^+e^-$  events that pass the above cuts are refit using a special form of the *BABAR* Kalman filter track fit which constrains the pair of tracks to have the same 4-momentum as the initial  $e^+e^-$  system, within the independently-estimated errors on the beam particle momenta. If the

$\chi^2$  of the pair fit is larger than 50, it is considered a failed fit, and the individual tracks in these events are passed down to the ‘normal’ track selection algorithm described below. The most common cause of failed pair fits is initial- and/or final-state radiation, which is not allowed for in the beam four-momentum constraint.

When successful, the *pair* fit of  $e^+e^- \rightarrow \mu^+\mu^-$  and  $e^+e^- \rightarrow e^+e^-$  events greatly improves the track momentum resolution. More importantly, the pair fit creates a correlated system in which information passes from one track through the IP to the other track. This allows the local alignment procedure to constrain the positions of wafers relative to those on opposite sides of the detector.

Because the *BABAR* track finding algorithm assumes all particle originate at or near the IP, a single cosmic ray passing through *BABAR* is initially reconstructed as two tracks, splitting the cosmic-ray trajectory through the detector roughly in half. Cosmic-ray event candidates are selected as having two well-measured oppositely charged tracks which match in angle and position at their point of closest approach to the IP. These tracks are also required to have associated calorimeter signals consistent with a minimum-ionizing particle. If these criteria are satisfied, the hits from the upward-going track are added to those on the downward-going track, and the combined track is refit. If the resulting combined track Kalman fit chi-squared consistency is better than 0.1, the event is retained as a cosmic ray.

Events which fail selection as  $e^+e^- \rightarrow \mu^+\mu^-$ ,  $e^+e^- \rightarrow e^+e^-$ , or cosmic-ray events are taken together with multi-track events as candidates for the ‘normal’ category. In this category, we select all the tracks which pass the usual selection cuts, plus an isolation cut. Any event with at least one selected track is classified as ‘normal’.

#### 4.5 Local alignment track selection and preparation

Selected tracks from events which pass final event selection in any category are themselves labeled according to their event category. In the case of ‘normal’ events, tracks are further categorized according to whether or not they have hits in adjacent wafers of the same layer in the *overlap* region (see Fig. 4.2). As these *overlap* tracks have a very short extrapolation distance between the hits in adjacent layers, they provide a particularly powerful statistical constraint, and so are especially valuable in the local alignment procedure. Non-*overlap* tracks in ‘normal’ events remain categorized as ‘normal’.

<sup>2</sup>The minimum so that the SVT information alone fully constrains all five track parameters.

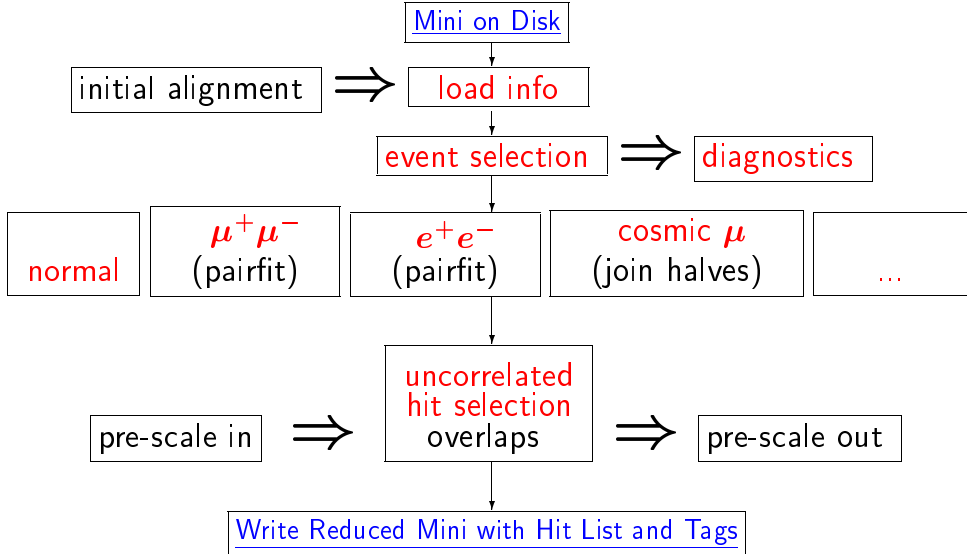


Fig. 4.4: Diagram of event/track/hit selection sequence

To balance the impact of the largely-independent global distortion systematic constraints afforded by the different track categories, we perform a final track selection which roughly equalizes the statistical power of the tracks in each category for every individual wafer. Because the wedge wafers (see Fig. 4.1) subtend a region of polar angle  $\theta$  where the rate from  $e^+e^- \rightarrow \mu^+\mu^-$  and other physics events changes rapidly with  $\theta$ , we further divide these into two roughly equal parts

We use a pseudo-random prescaling algorithm to select roughly 100 tracks from each category in every wafer. The pseudo-random algorithm is keyed on the unique event time, and so is fully repeatable but effectively random.

To allow better control of the propagation of systematic misalignment effects from the DCH into the SVT alignment tracks, we refit all tracks using the following technique. First, we split the tracks into two, one with all the SVT hits and one with all the DCH hits. Then, each of these associated but separate tracks are refit using the standard *BABAR* Kalman filter fit. The parameters and covariance matrix of the DCH-only track fit are sampled at the point where that track enters the SVT detector volume, and these parameters and covariance are then used to *constrain* the SVT-only track fit.

Mathematically, the parameter constraint is identical to the effect of having left the DCH hits on the track. However, by *masking* some of the parameters in the constraint, the information content of the DCH-only fit can be filtered. In particular, by masking off all but the  $\omega$  parameter (inverse curvature) of the DCH-only fit in the constraint, we can greatly improve the momentum resolution of the constrained SVT-only track, with-

out introducing any dependence on possible systematic distortions in the position or orientation of the DCH. We use the DCH-only fit  $\omega$  constraint when fitting the  $e^+e^- \rightarrow \mu^+\mu^-$ ,  $e^+e^- \rightarrow e^+e^-$ , cosmic-ray and overlap category tracks.

Because the sum of the local alignment parameters for all wafers include the six *global* degrees of freedom, the local alignment procedure could introduce a global *drift*. Because the  $\omega$  constraint does not depend on the relative position or orientation of the SVT and DCH it cannot constrain this global drift. To minimize the global alignment drift, we use all five DCH-only fit parameters to constrain the fit of the ‘normal’ tracks. As these tracks have the lowest statistical power, this introduces only a modest and acceptable dependence on DCH alignment distortions.

## 4.6 Hit selection

An ideal single track passing through all five layers of the SVT will generate one  $u$  and one  $v$  hit in each of five wafers. Because a track’s trajectory can be described with five parameters, by comparing the estimated extrapolation position of the track with the Si hit position in that wafer, each track can in principle constrain five degrees of freedom. Some of these constraints, however, are on the global position of the wafers, and the remainder are not the local (relative) positions we are interested in here.

Hits are selected in three stages. First, hits of questionable quality are disabled, and the tracks which held them are refit. Then the remaining hits are prescaled to give a uniform alignment sample over the

detector, the physics processes, and the time window in which the data sample was accumulated. Finally, once the alignment is close to convergence, an outlier removal cut is applied.

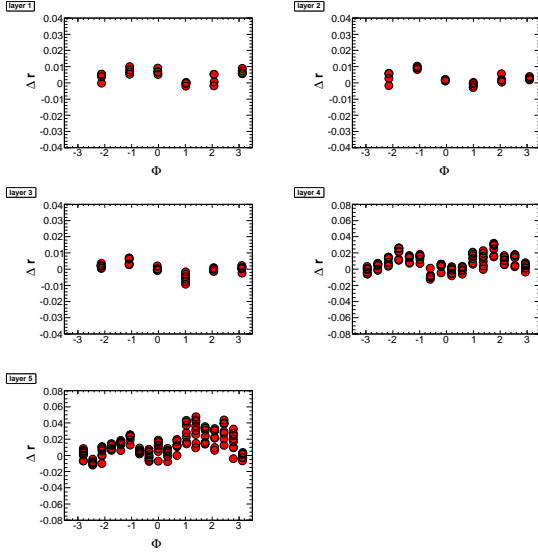


**Fig. 4.5:** Azimuthal angle  $\phi$  (rad) dependence of the radial difference ( $\Delta r$ , cm) of SVT wafer positions between the measured (to the best of our knowledge) and the optical survey geometry in (a) layer 1, (b) layer 2, (c) layer 3, (d) layer 4, and (e) layer 5. Each point represents the position of a wafer as measured in November 1999.

## 4.7 The optical survey constraint

In addition to the information from tracks, data from an optical survey performed during the assembly of the SVT are included in the alignment procedure. The typical precision of these optical measurements is  $4 \mu\text{m}$ . This survey information is only used to constrain wafers relative to other wafers in the same module, and not one module to another or one layer to another. Furthermore, only degrees of freedom in the plane of the wafer are constrained as they are expected to be the most stable, given the assembly procedure.

We illustrate the wafer positions as measured with track data (using the procedure discussed in this paper) compared to the optical survey measurement in Fig. 4.5. The overall double-sine wave is attributed to motion of modules during the detector installation. However, the relative positions of wafers within modules are well preserved after the module survey.

To add survey information to the alignment procedure, we treat the survey measurement of a given module as a ‘track’ and construct an unbiased residual for each wafer in a given module. This unbiased residual enters the full  $\chi^2$  for each module along with other

information from the charged track residuals.

The optical survey residual calculation works as follows. For each survey unit (e.g., module) we have  $N$  wafers ( $i = 1, \dots, N$ , e.g.,  $N = 8$  in layer five). Each wafer is represented by  $n$  points ( $j = 1, \dots, n$ , we chose  $n = 4$ ) with effective weight ‘mass’  $m_{ij}$  and global position  $\vec{r}_{ij}$  of each point. Each wafer position in either survey measurement or the current detector model is parameterized as a small displacement with respect to ideal geometry taken in local coordinates. The difference between these two small displacements corresponds to the small difference  $d\vec{r}_{ij}$  in global position of each point  $m_{ij}$  in a given wafer.

For any given wafer in a unit (e.g., module), we calculate the global transformation (translation  $\vec{R}$  and rotation  $\vec{\Omega}$ ) between the unit position in the survey measurement and the unit position in the current detector model. In order to obtain an unbiased residual, we exclude the wafer under consideration ( $i = I$ ) from this transformation. The values of  $\vec{R}$  and  $\vec{\Omega}$  are found in the formalism of rigid body motion which we adapt to our task, see Eqs. (4.1) and (4.2):

$$\left( \sum_{j,i \neq I}^{n \times N} m_{ij} \right) R_k = \left( \sum_{j,i \neq I}^{n \times N} m_{ij} \cdot d\vec{r}_{ij} \right)_k. \quad (4.1)$$

$$\begin{aligned} \sum_{k=1}^3 \Omega_k \sum_{j,i \neq I}^{n \times N} m_{ij} (\delta_{kl} (\vec{r}_{ij})^2 - (\vec{r}_{ij})_k (\vec{r}_{ij})_l) \\ = \sum_{j,i \neq I}^{n \times N} m_{ij} (\vec{r}_{ij} \times d\vec{r}_{ij})_l. \end{aligned} \quad (4.2)$$

After the global transformation  $\vec{R}$  and  $\vec{\Omega}$ , we effectively overlay the survey measurement on the current detector model. For each wafer under consideration, we find the difference in its position between the detector model and the reference survey adjusted globally as discussed above. This could be done easily with the same calculation in Eqs. (4.1) and (4.2) where we reverse the requirement from  $i \neq I$  to  $i = I$ . The resulting  $\vec{R}_I$  and  $\vec{\Omega}_I$  represent the unbiased residuals of each wafer in a module with respect to survey information. Their derivatives are calculated by adjusting the displacement size. The errors on the residuals are taken from the expected precision of the survey measurements discussed above. We apply an additional weight factor to the expected errors to account for time dependence and increase the errors by a factor of ten for the out-of-plane degrees of freedom (translation in  $w$  and rotation in  $u$  and  $v$ ).

The relative weights of the points  $m_{ij}$  provide additional flexibility in the procedure. We assign equal weight to each point within a module, except that we assign zero weight to the points on the wafers more than

distance  $R$  away from the wafer under consideration. This distance  $R$  was optimized to reduce the effect of too distant wafers and was chosen to be  $X$  cm.

The above procedure is then used in the  $\chi^2$  minimization procedure along with the charged track residuals, as discussed in the next section. Including the survey information as additional term in  $\chi^2$  provides the advantage of constraining certain degrees of freedom in the wafer positions, such as  $z$ -scale of the modules, while leaving them flexible enough for adjustment when charged track information dominates. This procedure may be found crucial at initial stages of a new experiment when only limited information from charged tracks is available.

The survey constraint could introduce a bias into the alignment if the Lorentz shift of wafers in a module are not the same. We have not studied this effect, but we estimate it to be small (at most a few microns).

#### 4.8 Minimization procedure used in the alignment

After all the above selections, a  $\chi^2$  is formed for each wafer by adding all the information for that wafer from each track (or survey measurement) across all the selection categories. Derivatives of this  $\chi^2$  with respect to the wafers's six local parameters are calculated numerically by evaluating the effect of small changes in those parameters on the residuals used in the  $\chi^2$ . The  $\chi^2$  for

each wafer is then minimized by solving analytically the matrix equation resulting from setting the derivative of  $\chi^2$  with respect to the alignment parameters to 0. Each wafer's  $\chi^2$  is minimized independently, and the changes in alignment parameters are stored.

To account for the dependence of the constraints on one wafer to the position of the others, the minimization procedure is iterated. This involves refitting all tracks and recomputing the survey constraint using the new alignment parameters solved for in the previous iteration.

Convergence for the minimization iteration is defined by looking at the change in alignment parameters of each wafer. A wafer is said to have converged when its parameters don't change by more than a few microns between iterations. The entire procedure is said to converge when all wafers are converged.

The alignment iterations are run on dedicated reduced data samples containing selected prescaled data, written in the reduced mini event format. An iteration over  $200 \text{ pb}^{-1}$  of selected data takes roughly 5 cpu-minutes on a 1 GHz Linux machine, and the iterative procedure typically converges after 100 iterations. Iteration bookkeeping, diagnostics, input/output and job management are controlled using a TCL-based interactive GUI. Figure 4.6 shows the iteration sequence.

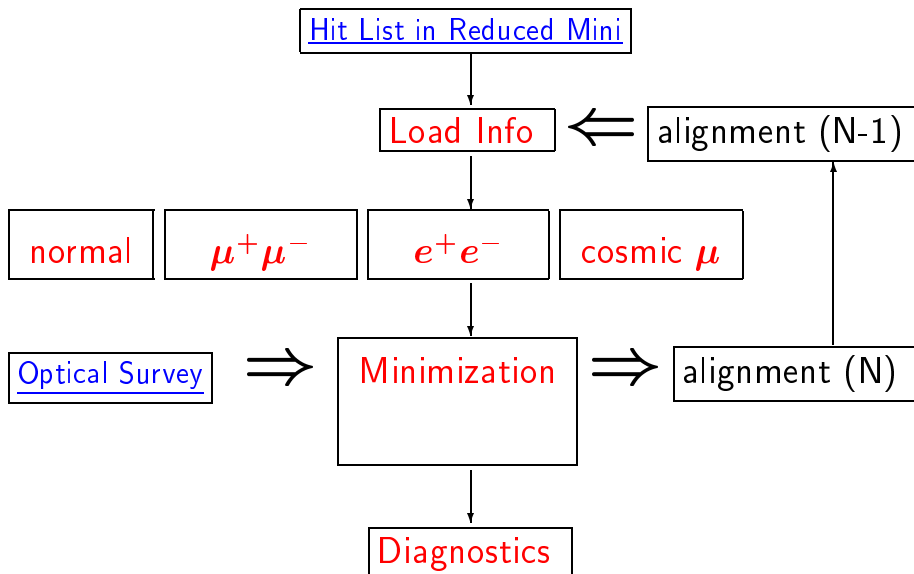
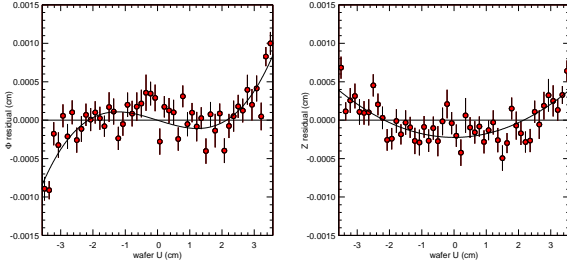


Fig. 4.6: Diagram of iteration sequence

## 4.9 Description and fitting of SVT wafer curvature

During initial tests of the local alignment algorithm using the real data we observed some internal inconsistencies. First of all, overlap hit residuals were somewhat biased indicating radial bias. Closer investigation of hit residuals as a function of local wafer coordinates revealed strong local azimuthal dependence, but not  $z$  dependence. See Fig. 4.7 for illustration of  $\phi$  and  $z$  hit residual bias.



**Fig. 4.7:** Hit residual measurements for the  $\phi$  (left) and  $z$  (right) SVT wafer readouts in layer three as a function of local coordinates in azimuthal ( $u$ ) direction

One basic assumption in SVT alignment was flat geometry of individual wafers. While SVT wafers are constraint by ribs in the  $z$  direction, it might be possible to have curvature in orthogonal direction with sagitta  $S < 100 \mu\text{m}$ . This effect should be more important in the inner layers where the width ( $2L$ ) of the wafers is larger, especially in layer three. If we define the curvature of a wafer with the radius  $R$ , then:

$$C = 1/R = 2S/L^2 . \quad (4.3)$$

This wafer curvature hypothesis is consistent with the bias observed in Fig. 4.7. We can define geometric bias of wafer position as a function of local azimuthal coordinate  $u$ :

$$\Delta r(u) = (u^2 - u_0^2)/2R , \quad (4.4)$$

where  $u_0$  is the parametrization of the global position. We have  $u_0 = L/\sqrt{3}$  for the global position preserving centre of gravity. It follows that the hit residual bias  $\Delta P$  as a function of  $u$  would be:

$$\begin{aligned} \Delta P &= \sin(\alpha) \times \Delta r(u) \\ &= \sin(\alpha) \times (u^2 - u_0^2)/2R \\ &= f(u)/R , \end{aligned} \quad (4.5)$$

where the angle  $\alpha$  is defined as the angle between the normal to the wafer and the track projection orthogonal to the hit (read-out strip). For the  $\phi$  hit  $\sin(\alpha)$  is approximately  $u/r$ , while for the  $z$  hit  $\alpha$  is approximately the

dip angle of the wafer (for the high-momentum tracks coming from the origin). This explains both plots in Fig. 4.7 where we use Eq. (4.5) with the approximation above in the fit.

We should note that no curvature effects were observed in Monte Carlo simulation (which is known to have perfect flat wafer geometry) and additional evidence for the correct interpretation of results comes from alignment validation to be discussed later.

Since wafer curvature appears to be important, we implement this in the Detector Model with exact parabolic displacement according to Eq. (4.4) for the  $\phi$  read-out strips and approximate piece-wise shape for the  $z$  read-out strips as shown in Fig. 4.8. We chose  $u_0 = 0$  for simplicity of the Detector Model parametrization to be used in alignment procedure.

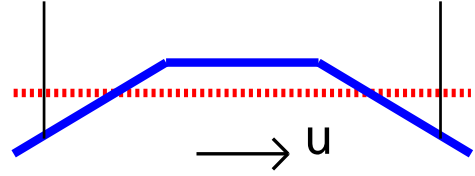


**Fig. 4.8:** Piece-wise wafer curvature model for the  $z$  read-out strips

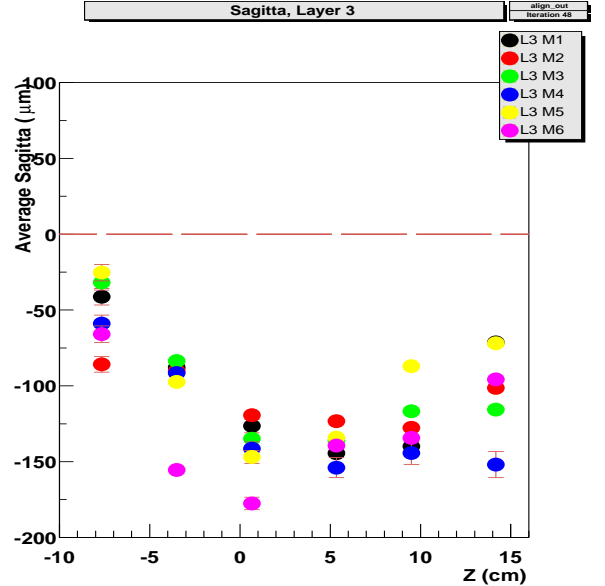


**Fig. 4.9:** Results of the fits for the wafer sagitta in layer three (the vertical scale is wrong by a factor of two in this version)

In the alignment procedure we compute the  $\chi^2$  to be minimized with respect to the individual wafer curvature:

$$\chi^2 = \sum_{\phi \text{ hits}} (\Delta P_\phi - f_\phi(u) \times C)^2 / \sigma_{P_\phi}^2 + \sum_{z \text{ hits}} (\Delta P_z - f_z(u) \times C)^2 / \sigma_{P_z}^2. \quad (4.6)$$

We require the  $\chi^2$  derivative to be zero and solve the equation analytically. In the alignment job we accumulate the necessary sums over all the hits and compute the most probable curvature value of  $C$  for each wafer. In Fig. 4.9 we illustrate the results of the sagitta calculations for different wafers in layer three. Strong dependence on the  $z$  wafer position is observed.

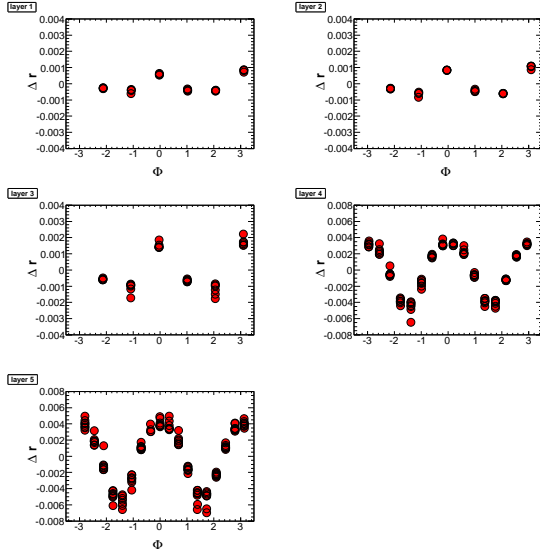
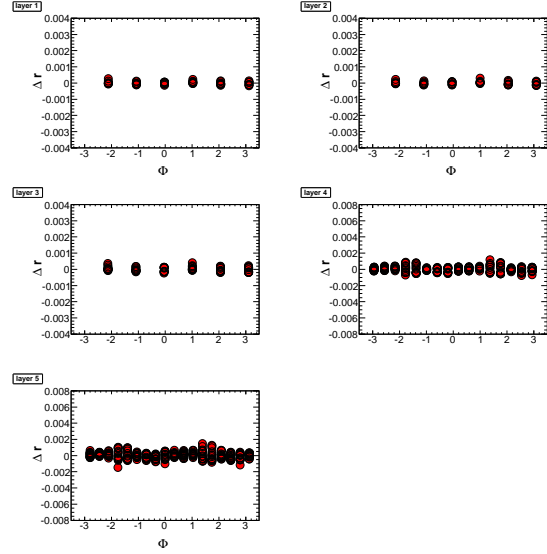


**Fig. 4.10:** Azimuthal angle  $\phi$  (rad) dependence of the radial difference ( $\Delta r$ , cm) of SVT wafer positions after elliptical deformation. (a) layer 1, (b) layer 2, (c) layer 3, (d) layer 4, and (e) layer 5. Each point represents the position of a wafer.

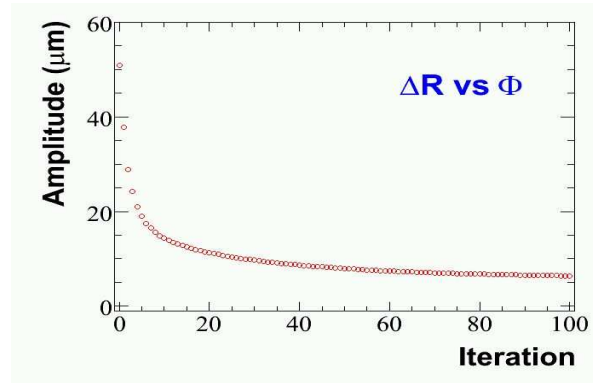
#### 4.10 Validation tests of the alignment

We test the ability of the local alignment procedure to remove systematic distortions by introducing a coherent misalignment of the SVT the wafers, and then running the alignment procedure taking that misalignment as the initial condition. These global distortions are particularly difficult to remove as the residuals used in the alignment procedure typically depend on them only to second order. An example of a distorted initial condition is where the radius of the wafers is varied as  $\cos \phi$ , resulting in an elliptical shape, as shown in Fig. 4.10. We test nine distinct distorted initial conditions, as described in Table 4.2. To correspond to realistic con-

ditions, we set the initial scale of these distortions to  $50 \mu\text{m}$ .



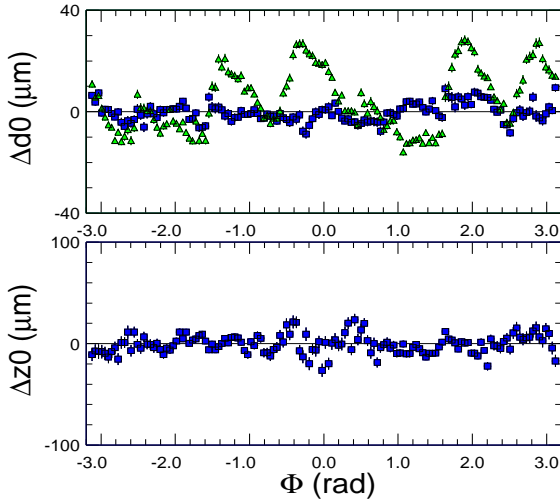
**Fig. 4.11:** Azimuthal angle  $\phi$  (rad) dependence of the radial difference ( $\Delta r$ , cm) of SVT wafer positions after the alignment procedure has converged, starting with the elliptical deformation shown above as initial condition. (a) layer 1, (b) layer 2, (c) layer 3, (d) layer 4, and (e) layer 5. Each point represents the position of a wafer.



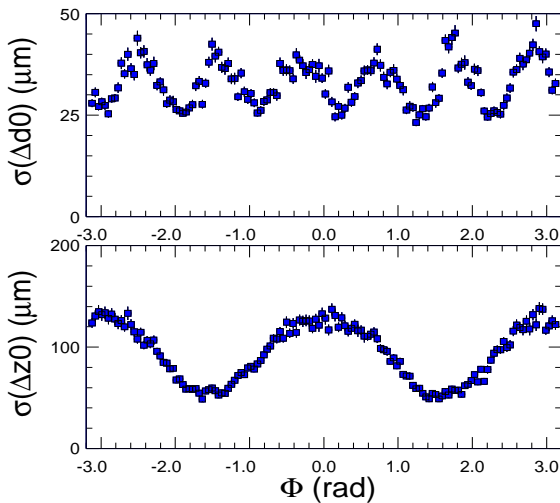
**Fig. 4.12:** Amplitude of the remaining elliptical distortion as a function of iteration during the alignment procedure starting with the  $50 \mu\text{m}$  amplitude elliptical distortion initial condition described above

Figure 4.11 shows the wafer positions in the relevant projection when the alignment procedure has run to convergence after starting with the elliptical distortion described above. This is a typical result, showing a residual distortion of a few  $\mu\text{m}$  amplitude, which is

within the goals of the procedure. To study the convergence of the alignment procedure we fit for the amplitude of the distortion remaining as a function of iteration, as shown in Fig. 4.12 for the elliptical distortion. This rate of convergence is typical. In all cases we find the alignment procedure is capable of reducing global distortions to a negligible level.



**Fig. 4.13:** Best achieved dimuon track mismatch  $d0$  (top) and  $z0$  (bottom) for 12-series alignment. Squares show 12-series validation (P-type alignment), while triangles show 10-series alignment processing for comparison (N-type alignment from September 2000).



**Fig. 4.14:** Impact-parameter resolution with dimuon tracks  $d0$  (top) and  $z0$  (bottom) for 12-series alignment. The resolution in  $z0$  is dominated by beamspot position uncertainty in the  $x$  direction.

Our confidence in the SVT local alignment performance also comes from validation tests done with the physics events. However, most of the high-level validation tests require large statistics and the only practical samples of events used for the fast monitoring are dimuon and cosmic tracks. Even if the same data were used for alignment production, the samples are essentially statistically independent owing to the high prescaling used in the alignment procedure. Additionally, we use beamspot position constraint in the validation which provides additional information. Examples of dimuon mismatch measurements are shown in Figs. 4.13 and 4.14. Two important improvements were achieved with the latest alignment: better constraint on elliptical distortion (otherwise visible as double sine wave in 10-series) and better radial scale constraint due to wafer curvature measurements (otherwise visible as six-fold structure in 10-series).

The other important validation test of the local alignment is the mismatch of two halves of a cosmic track. Both tracks should have identical parameters in the origin if assumed to be independent.

## Acknowledgements

The work presented in this note could not have been accomplished without the help of many people. Many of the ideas for this procedure were inspired by the first *BABAR* SVT alignment procedure developed by Jochen Schieck. We also wish to thank Stefan Kluth, Amir Farbin, Vincent Lillard, Gennadiy Kukartsev, Jurgen Krosberg, Chung Khim Lae, Luke Winstrom, and Zijin Guo for actually generating the alignment constants ultimately used in physics analysis. We also wish to thank Eric Charles and Fred Goozen for providing the optical survey measurements, the SVT group for building and operating this beautiful detector, the tracking group for their support with validation studies, and *BABAR* and PEP-II for providing the data.

## References

- [1] D. Brown, for the *BABAR* Collaboration, *The new BABAR analysis model*, CHEP 2004 presentation 347.
- [2] I. Gaponenko, for the *BABAR* Collaboration, *CDB - Distributed Conditions Database of BaBar experiment*, CHEP 2004 presentation 316.
- [3] J.K. Ousterhout, *Tcl and the Tk Toolkit* (Addison-Wesley, Reading, MA, 1994).
- [4] D. Brown *et al.*, *The BABAR track fitting algorithm*, presented at CHEP2000.
- [5] *BABAR* Collaboration, SLAC-R-95-457.
- [6] *The BABAR prompt reconstruction system*, presented at CHEP97.